

Revisiting Constraints on Primordial Curvature Power Spectrum from PBH Abundances

Ashu Kushwaha^a and Teruaki Suyama^a

^aDepartment of Physics, Institute of Science Tokyo, 2-12-1 Ookayama, Meguro-ku, Tokyo 152-8551, Japan

E-mail: kushwaha.a.ce1b@m.isct.ac.jp, suyama@phys.sci.isct.ac.jp

Abstract. Primordial black holes (PBHs) can form in the early Universe, for instance during radiation domination, from the collapse of large-amplitude density perturbations shortly after horizon re-entry. This mechanism establishes an approximate one-to-one correspondence between the PBH mass and the scale of the peak in the primordial curvature perturbations. Consequently, the constraints on PBH abundances can be translated into upper limits on the amplitude of the primordial curvature power spectrum, thereby providing an indirect probe of the last e-folds of inflation corresponding to these smaller scales. We derive constraints on the amplitude of primordial curvature power spectra with both narrow and broad peaks using the most up-to-date bounds on PBH abundances. Given the theoretical uncertainties in PBH formation, we systematically compare the constraints obtained using the Press–Schechter (PS) formalism and peak theory, accounting for the nonlinear relation between curvature perturbations and density contrast. We quantify the impact of spherical versus non-spherical collapse criteria and show that including non-sphericity significantly increases the inferred amplitude of the primordial power spectrum, reflecting the larger threshold density contrast required for PBH formation. We also find that whereas the constraints obtained using the PS formalism and peak theory remain largely similar for the monochromatic case, they differ significantly toward smaller scales in the case of a broad primordial power spectrum. This discrepancy underscores that current constraints remain sensitive to the choice of statistical formalism. Our consistent treatment of monochromatic and extended mass functions provides a systematic mapping based on existing methodologies, while highlighting that reducing these theoretical uncertainties is a crucial step toward probing the early Universe through PBHs.

Contents

1	Introduction	1
2	The compaction function and criterion for the collapse of an overdense region: A brief review	2
2.1	Equivalence between compaction function and averaged (smoothed) density contrast	3
2.2	Effect of non-sphericity of the overdense region	5
3	PBH mass function: A brief review	6
3.1	Definition of the PBH mass function	6
3.2	PBH mass function and the mass fraction parameter β	6
3.3	Mass fraction parameter in PS formalism	7
3.4	Mass fraction parameter in the peak theory	8
3.5	PBH mass in the critical phenomena	8
4	Constraints on $\mathcal{P}_\zeta(k)$ from PBHs abundance	9
4.1	Constraints on narrow peaked power spectrum from monochromatic PBH mass function	9
4.2	Constraints on broad peaked power spectrum from extended PBHs mass function	11
5	Conclusion	15
A	Calculations on relating volume average density contrast with smoothed density contrast	15

1 Introduction

Cosmic microwave background (CMB) and large-scale structure (LSS) observations have established the amplitude of primordial curvature perturbations on cosmological scales with high precision, thereby placing strong constraints on inflationary models [1, 2]. These measurements, however, probe only a limited range of comoving scales (for example, $10^{-4} \text{ Mpc}^{-1} \lesssim k \lesssim 0.01 \text{ Mpc}^{-1}$), leaving the properties of primordial perturbations on much smaller scales essentially unconstrained by direct observations.

Primordial fluctuations on small scales are nevertheless of particular interest, since they encode information about the final stages of inflation. At present, the most stringent constraints on such small-scale perturbations arise from the non-detection of primordial black holes (PBHs). If the amplitude of primordial fluctuations were sufficiently large (which can be achieved by introducing nontrivial physics during inflation, see Refs. [3, 3–14]), PBHs would be produced abundantly in the early Universe [15–25]. The absence of observational evidence for PBHs therefore allows one to place upper bounds on the amplitude of the primordial curvature power spectrum on scales far smaller than those accessible to CMB and LSS observations.

Since PBHs are formed shortly after the horizon re-entry during the RD epoch, this provides an approximate one-to-one correspondence between the mass of the PBHs and the

scale of the peak in the primordial curvature perturbations during inflation. Interestingly, this connection allows us to translate the constraints from one to the other; for instance, we can constrain the primordial curvature power spectrum from the PBHs abundance, which is the primary focus of this work¹. This method has been investigated in the literature [27–29]. Due to the uncertainties associated with the PBHs’ formation mechanisms, the constraints on the primordial power spectrum are also affected, which requires more refined calculations by a systematic treatment of potential sources of uncertainties. For example, the formation of PBHs has been broadly discussed within the context of Press-Schechter (PS) formalism [30] and Peak theory [31]. However, the estimation of the PBHs mass distribution (or the abundance of PBHs) differs between the two approaches [21, 32–34], and the preference for one over the other remains uncertain. Another important source of uncertainty is the correct prescription of the shape of the overdense region, which is often considered to be spherical; however, it is shown that the threshold density contrast increases for an ellipsoidal overdense region, thus affecting the constraints [35].

In this work, we revisit the study of constraining the small-scale primordial curvature power spectrum from the PBHs abundance. By using the most updated constraints on PBHs abundance provided in Ref. [22], we perform a systematic study of various issues leading to the uncertainties in the estimation of PBHs abundance. Specifically, using the refined calculations based on the compaction function, with the non-linear relation between density contrast and curvature perturbation and including non-sphericity of the overdense region, we compare the constraints for the following cases: (i) PS formalism with Peak theory, (ii) monochromatic and extended mass distribution of PBHs. Note that some of these effects have been considered in the previous literature (see Refs. [27–29, 36–38], however, to the best of our knowledge, all these effects have not been considered together to derive the constraints on the primordial curvature power spectrum. Therefore, the constraints obtained in this work may provide a better comparison and can be considered as more precise and robust. This work is organized in the following way: in section 2, we discuss the criterion for the collapse based on the compaction function. Section 3 discusses the methodology to compute the PBHs abundance, and in section 4 we provide the final constraints on the power spectrum. Section 5 provides the summary.

2 The compaction function and criterion for the collapse of an overdense region: A brief review

In this section, we provide a brief review of the criterion for the collapse of an overdense region into PBHs, based on earlier studies [28, 39, 40], which will be used in the subsequent analysis. Let us consider a spacetime where superhorizon-scale spherically symmetric overdense region is superposed on top of the flat Friedmann–Lemaître–Robertson–Walker (FLRW) universe. The metric of this spacetime is given by

$$ds^2 = -dt^2 + a^2(t)e^{2\zeta(r)} [dr^2 + r^2 d\Omega^2] \quad (2.1)$$

where $a(t)$ is the scale factor in cosmic time t , $\zeta(r)$ is the curvature perturbation, r is the radial coordinate which is related to the physical radius (or areal radius) as $R(r, t) = a(t)re^{\zeta(r)}$. The local overdensity (or density contrast) of a region of radius r centered at a point \mathbf{x} is defined as

¹Similarly, we can constrain the power spectrum of primordial magnetic fields during the RD epoch from the abundance of PBHs, see Ref.[26] for more details.

$\frac{\delta\rho(r,t,\mathbf{x})}{\bar{\rho}(t)} = \frac{\rho(r,t,\mathbf{x}) - \bar{\rho}(t)}{\bar{\rho}(t)}$, where $\rho(r,t,\mathbf{x})$ is the energy density of the overdense region, $\bar{\rho}(t) = \frac{3H^2}{8\pi}$ is the background energy density and $H(t) = \dot{a}/a$ is the Hubble parameter.

In the gradient expansion formalism, the non-linear relation between the density contrast $\delta\rho/\bar{\rho}$ (defined on a comoving uniform-cosmic time slicing) and the curvature perturbation ζ is given by [28, 39–41]

$$\frac{\delta\rho(r,t)}{\bar{\rho}(t)} = -\frac{4(1+w)}{5+3w} \left(\frac{1}{aH}\right)^2 e^{-5\zeta(r)/2} \nabla^2 e^{\zeta(r)/2} \quad (2.2)$$

where $w = p/\rho$ is the equation of the state parameter, which is 1/3 for the RD era. Thus, the non-linear density contrast becomes

$$\frac{\delta\rho}{\bar{\rho}} = -\frac{2(1+w)}{5+3w} \left(\frac{1}{aH}\right)^2 e^{-2\zeta(r)} \left[\zeta''(r) + \frac{2}{r}\zeta'(r) + \frac{1}{2}\zeta'(r)^2 \right]. \quad (2.3)$$

We used for spherically symmetric system $\nabla^2 e^{\zeta(r)/2} = \frac{1}{2}e^{\zeta(r)/2} \left[\zeta''(r) + \frac{2}{r}\zeta'(r) + \frac{1}{2}\zeta'(r)^2 \right]$, where $' = \frac{d}{dr}$. At linear order, the above equation gives

$$\frac{\delta\rho}{\bar{\rho}} \simeq -\frac{2(1+w)}{5+3w} \left(\frac{1}{aH}\right)^2 \left[\zeta''(r) + \frac{2}{r}\zeta'(r) \right]. \quad (2.4)$$

Note that the density contrast $\delta\rho/\bar{\rho}$ is a local quantity and is defined at a given location. However, PBH formation is determined by whether the region as a whole is sufficiently overdense when it re-enters the horizon, which depends on the total mass excess enclosed within a finite volume rather than on the local density contrast. It is therefore more useful to consider the volume-averaged density contrast within a sphere of areal radius R , which directly captures this condition. This quantity is defined as

$$\delta(r,t) = \frac{1}{V} \int_0^R dR 4\pi R^2 \frac{\delta\rho}{\bar{\rho}} \quad (2.5)$$

where $V = 4\pi R^3/3$.

2.1 Equivalence between compaction function and averaged (smoothed) density contrast

In recent years, the compaction function has become a popular quantity in calculating PBH abundance. As compared to the average density contrast, the compaction function allows us to consistently determine the correct radius (length scale) of the overdense region and compare the curvature and overdensity profiles with different shapes. The compaction function quantifies the magnitude of the gravitational potential and is defined as twice the ratio between the mass excess δM inside a sphere of areal radius $R(r,t)$ at a time t to the areal radius itself as² [28, 40, 43–46]

$$C(r,t,\mathbf{x}) \equiv \frac{2\delta M(r,t,\mathbf{x})}{R(r,t,\mathbf{x})}, \quad (2.6)$$

where $\delta M(r,t,\mathbf{x}) = M(r,t,\mathbf{x}) - \bar{M}(t)$ is the excess mass within a sphere of areal radius $R(r,t,\mathbf{x})$ centered at the point \mathbf{x} and $\bar{M}(t) = \frac{4\pi R^3(r,t)}{3}\bar{\rho}(t)$ is the mass corresponding to

²The compaction function was introduced by Shibata and Sasaki [42] as $C = \delta M/R$.

the background energy density. One important feature of the compaction function is that it is conserved on superhorizon scales, where $H(t)R(r, t) \gg 1$. Therefore, we can take the compaction function as a time-independent quantity before the horizon crossing time t_{hc} . The length scale of the perturbation (i.e., the radius of the overdense region) can be determined by the location r_m of the local maxima of the compaction function as $C'(r_m) = 0$, see Refs. [40, 43]. Because the maxima of the compaction function (measured by $2M/R$) directly corresponds to the maxima of the Newtonian gravitational potential (measured by M/R), r_m gives the correct and physically well-motivated estimation of the radius of the overdense region.

Let us first calculate the mass excess as the volume integral of excess density with a sphere of physical radius R_m corresponding to the location of maxima of the compaction function i.e., r_m as

$$\delta M(R_m, t) = M(R_m, t) - \bar{M}(t) = \bar{\rho} \int_0^{R_m} dR 4\pi R^2 \frac{\delta\rho}{\rho} . \quad (2.7)$$

Using the non-linear relation (2.3) for $\delta\rho/\bar{\rho}$ in the above equation gives the compaction function (2.6) for the non-linear relation as [28, 43]

$$C_{\text{NL}}(r_m) = -\frac{3(1+w)}{5+3w} r_m \zeta'(r_m) [2 + r_m \zeta'(r_m)] . \quad (2.8)$$

Similarly, the compaction function for the linear relation (2.4), can be given as

$$C_L(r_m) = -\frac{6(1+w)}{5+3w} r_m \zeta'(r_m) . \quad (2.9)$$

Note that the subscripts L and NL refer to the linear (2.4) and non-linear relations (2.2) between the curvature perturbation ζ and density contrast $\delta\rho/\bar{\rho}$. Using Eq.(2.9) in Eq.(2.8) allows us to obtain the non-linear compaction function in terms of the linear component as

$$C_{\text{NL}} = C_L - \frac{1}{12} \left(\frac{5+3w}{1+w} \right) C_L^2 = C_L - \frac{3}{8} C_L^2 \quad (2.10)$$

where in the last expression we used $w = 1/3$ for the RD era. The above equation suggests that C_{NL} is maximum at $C_L = 4/3$ with $C_{\text{NL,max}} = 2/3$.

From the definitions of δ and C , it follows that $C_{\text{NL}}(r_m) = H^2 R_m^2 \delta(r_m, t)$. Thus, we can identify $C_{\text{NL}}(r_m)$ with the smoothed density contrast evaluated at the horizon reentry time $HR_m = 1$. Denoting by δ_L the linear part of $\delta_m(r_m, t_{hc})$, where t_{hc} is the horizon reentry time of the scale r_m , Eq. (2.10) gives

$$\delta_m = \delta_L - \frac{3}{8} \delta_L^2, \quad (2.11)$$

where $\delta_m \equiv \delta_m(r_m, t_{hc})$. The LHS of the above equation can be associated with the threshold density contrast of PBHs formation (δ_c), and we will refer this as $\delta_{m,c}$. Solving for the roots of the above quadratic equation gives the corresponding threshold value of the linear component $\delta_{L,c}$ as

$$\delta_{L\pm,c} = \frac{4}{3} \left(1 \pm \sqrt{1 - \frac{3}{2} \delta_{m,c}} \right) . \quad (2.12)$$

One can see that for a typical value of the threshold density contrast, $\delta_c = 0.45 = \delta_{m,c}$, the root $\delta_{L+,c} = \frac{4}{3} \left(1 + \sqrt{1 - \frac{3}{2}\delta_{m,c}} \right) \simeq 2.09$ corresponds to very large amplitude perturbations referred to as the type-II perturbations. For the Gaussian primordial fluctuations, the contribution of PBHs abundance from the type II fluctuations is typically suppressed. Recently, Ref.[47] studied the numerical simulation of type II fluctuations, showing that they do not necessarily result in type II PBHs during RD epoch. Therefore, in the following, we focus on type-I PBHs and consider the physically relevant root $\delta_{L-,c}$. This threshold incorporates the nonlinear relation between the density contrast and the curvature perturbation while allowing us to work with the linear density contrast δ_L . Because δ_L is linearly related to the curvature perturbation ζ , the statistical properties of δ_L are the same as those of ζ . For later purpose, we provide the linear relation in Fourier space obtained by combining Eq. (2.4) and the linearized Eq. (2.5):

$$\tilde{\delta}_L(\mathbf{k}, t) = \frac{2(1+w)}{5+3w} \frac{k^2}{a^2 H^2} \tilde{W}(k, R) \tilde{\zeta}_{\mathbf{k}}, \quad (2.13)$$

where $\tilde{W}(k, R)$ is the Fourier transform of the top-hat Window function $W(r, R) = \Theta(R - r)$ and is given by

$$\tilde{W}(k, r_m) = 3 \frac{\sin(kr_m) - kr_m \cos(kr_m)}{(kr_m)^3} = 3 \frac{j_1(kr_m)}{kr_m}, \quad (2.14)$$

and j_1 is the spherical Bessel function.

2.2 Effect of non-sphericity of the overdense region

The overdense region in more realistic scenarios is not perfectly spherical; therefore, to precisely estimate the threshold density contrast, the non-sphericity should be taken into account. The non-spherical overdense region can be modeled as an ellipsoid, for which the threshold density contrast is given by $\delta_{ec} \simeq \delta_{sp}(1 + 3e)$, where $e \simeq \frac{3\sigma}{\sqrt{10\pi}\delta}$ is the ellipticity and δ_{sp} is the threshold for the spherical overdensity [21, 35, 48, 49]. This relation suggests that a larger threshold density contrast is needed for ellipsoidal overdense regions to form PBHs as compared to spherical shapes. To incorporate this effect in our analysis, we use Eq.(2.11) which allows us to obtain the threshold density contrast for ellipsoidal collapse as

$$\delta_{ec} \simeq \delta_{L-,c} \left(1 + \frac{9\sigma_L}{\sqrt{10\pi}\delta_{L-,c}} \right). \quad (2.15)$$

Because, the effect of non-linearity between δ and ζ has not been studied to estimate the threshold density contrast for the ellipsoidal overdense region, we work with linear relation in the above equation and ignore the non-linear terms from the full expression. We anticipate that this approximation would not affect our constraint significantly. Although this estimation is not strictly correct because all the relations are obtained by assuming a spherically symmetric overdense region. However, deriving the relations for the nonspherical overdense region is very complicated, and we believe using δ_{ec} given in Eq.(2.15) as the threshold density contrast for the ellipsoidal collapse would provide a good comparison of the PBHs abundance estimation between the spherical and non-spherical cases.

3 PBH mass function: A brief review

In this section, we provide a brief overview of computing the PBH mass function from the primordial curvature perturbation, following earlier works [21]. Throughout this work we restrict ourselves to Gaussian curvature perturbations, and neglect the effects of primordial non-Gaussianity.

3.1 Definition of the PBH mass function

We define the PBH mass function $\psi(M)$ such that $\psi(M)dM$ represents the mass fraction of PBHs whose masses are in the infinitesimal mass range $(M, M + dM)$ with the normalization factor set by total dark matter abundance

$$\int dM \psi(M) = f_{\text{PBH}}. \quad (3.1)$$

Here $f_{\text{PBH}} \equiv \frac{\Omega_{\text{PBH}}}{\Omega_{\text{CDM}}}$ is the fraction of PBHs in dark matter and $\Omega_{\text{CDM}} = 0.265$ is the matter density parameter at the present epoch. We emphasize that this definition of the PBH mass function is independent of the PBH formation mechanism.

3.2 PBH mass function and the mass fraction parameter β

To constrain the primordial power spectrum from the abundance of PBHs, we need to obtain the relation between the PBH mass function and primordial power spectrum. However, this relation is inherently ambiguous, since no proposed method provides a rigorous first-principles derivation of the PBH mass function. As a result, one must rely on phenomenological approaches motivated by physical intuition, leading to several approximate and mutually incomplete expressions for the mass function. In this paper, we adopt the postulate given in the literature [50] that the so-called mass fraction parameter usually denoted by $\beta(M)$, whose concrete expression will be given later, represents the mass fraction of PBHs evaluated at their formation time in the logarithmic mass bin:

$$\Omega_{\text{PBH}} = \int \beta(M) \left(\frac{M_{\text{eq}}}{M} \right)^{\frac{1}{2}} d \ln M. \quad (3.2)$$

Here M_{eq} is the horizon mass at the time of the matter-radiation equality and the factor $\left(\frac{M_{\text{eq}}}{M} \right)^{\frac{1}{2}}$ accounts for the fact that PBH abundance relative to radiation grows in proportional to the scale factor during the RD era. Comparing this relation with the definition of the mass function (3.1) immediately yields

$$\psi(M_{\text{PBH}}) = - \frac{2}{\Omega_{\text{CDM}} k_{\text{eq}}} \frac{dk_m}{dM_{\text{PBH}}} \beta(k_m), \quad (3.3)$$

where k_{eq} is the comoving wavenumber of perturbations that reenter the Hubble horizon at the time of the matter-radiation equality and $k_m = 1/r_m$ is related to the PBH mass M_{PBH} by $k_m = a_m/M_{\text{PBH}}$ (a_m is the value of the scale factor evaluated at the time when the scale r_m reenters the Hubble horizon). Notice that dk_m/dM_{PBH} is negative. In this framework, the computation of the PBH mass function boils down to the computation of $\beta(k_m)$, following

the relation ³

$$\psi(M_{\text{PBH}}) = \frac{1}{\Omega_{\text{CDM}}} \left(\frac{g_*}{10.75} \right)^{-1/12} \left(\frac{2.9 \times 10^5 \text{ Mpc}^{-1}}{k_{\text{eq}}} \right) \left(\frac{30 M_{\odot}}{M_{\text{PBH}}} \right)^{1/2} \left(\frac{1}{M_{\text{PBH}}} \right) \beta(M_{\text{PBH}}(k_m)) . \quad (3.4)$$

In the literature, there are two representative approaches that connect β to the primordial power spectrum. They are PS formalism and the peak theory. In what follows, we review how β is related to \mathcal{P}_{ζ} in each formalism.

3.3 Mass fraction parameter in PS formalism

In the PS formalism, the mass fraction parameter β is defined as [30]

$$\beta(k_m) = \int_{\delta_{L-,c}}^{\delta_{\text{max}}} d\delta_L \frac{M_{\text{PBH}}(\delta_L)}{M_H} P(\delta_L), \quad (3.5)$$

where δ_L is the density contrast smoothed over the scale $r_m = 1/k_m$, $\delta_{\text{max}} = 4/3$ is the maximum value of δ_L corresponding to the maxima $C_{L,\text{max}}$ and $P(\delta_L)$ is the probability distribution function (PDF) of δ_L . The PBH mass M_{PBH} depends on δ_L when the critical phenomena is taken into account (see 3.5) and M_H is the horizon mass when the scale $r_m = 1/k_m$ reenters the Hubble horizon. Often, a factor of ‘2’ is multiplied in the above formula following the original PS formalism [30], which is related to the ‘cloud-in-cloud’ problem. However, in our previous work [51], using the excursion set formalism, we have shown that the prescription of multiplying by the factor ‘2’ is not justified for computing the abundance of PBHs formed during the RD era. In this paper, we assume that the multiplication factor is one and adopt Eq. (3.5) to compute the PBH abundance. Although, for the purpose of constraining the primordial power spectrum from PBHs abundance, this multiplicative factor would approximately give the same results.

Because ζ is assumed to follow Gaussian statistics, δ_L is also Gaussian. Thus, the PDF of δ_L is given by

$$P(\delta_L) = \frac{1}{\sqrt{2\pi} \sigma_L} \exp\left(-\frac{\delta_L^2}{2\sigma_L^2}\right), \quad (3.6)$$

where $\sigma_L^2 = \langle \delta_L^2 \rangle$ is the variance of the density contrast δ_L and from Eq. (2.13), it is related to the primordial spectrum of ζ by

$$\sigma_L^2 = \frac{16}{81} \int_0^\infty \frac{dk}{k} (kr_m)^4 \tilde{W}^2(k, r_m) \mathcal{P}_{\zeta}(k) , \quad (3.7)$$

The PBH mass fraction is then given by

$$\beta(k_m) = \int_{\delta_{L-,c}}^{\delta_{\text{max}}} d\delta_L \left(\frac{M_{\text{PBH}}(\delta_L)}{M_H} \right) \frac{1}{\sqrt{2\pi} \sigma_L} \exp\left(-\frac{\delta_L^2}{2\sigma_L^2}\right) . \quad (3.8)$$

³Alternatively, we can also define $\psi(M)$ as dimensionless quantity by $\psi(M) = \frac{1}{\Omega_{\text{CDM}}} \frac{d\Omega_{\text{PBH}}}{d \ln M}$, such that $f_{\text{PBH}} = \int d \ln M \psi(M)$, see [29, 46]. One can also define the mass function as the derivative of the probability (i.e., $\beta(M)$), however, as it is shown in our previous work [51], this may lead to the negative PBH mass function (thus, unphysical) in certain mass ranges. Since no method currently provides a rigorous first-principles derivation of the mass function. As a result, one should rely on phenomenological approaches motivated by physical intuition, yielding several approximate, mutually incomplete expressions for the mass function.

As we can see from the above equation, the PBH mass fraction is related to the primordial curvature power spectrum $\mathcal{P}_\zeta(k)$ via the variance σ_L^2 in Eq.(3.7). Therefore, given the constraints on PBHs' abundance, we can invert the above equation to constraints on $\mathcal{P}_\zeta(k)$.

3.4 Mass fraction parameter in the peak theory

The peak theory is based on the assumption that the peaks in smoothed linear density field δ_L correspond to peaks in smoothed nonlinear density field such that $\delta_m = C_{\text{NL}}$, where C_{NL} in Eq.(2.8) can be applied to calculate the height of the peaks in nonlinear field (although this statement may not be true in general, but will be valid in the case that only sufficiently rare and large peaks are considered, see Ref. [40]). The mass fraction parameter β is related to the number density of the peaks as

$$\beta(k_m) = \frac{(2\pi)^{3/2}}{(aH)^3} \int_{\delta_{L-,c}}^{\delta_{\text{max}}} d\delta_L \frac{M_{\text{PBH}}(\delta_L)}{M_H} n\left(\frac{\delta_L}{\sigma_L}\right), \quad (3.9)$$

where $(aH)^{-1}$ is the horizon size at the re-entry⁴. The number density $n\left(\frac{\delta_L}{\sigma_L}\right)$ for a random Gaussian field of rare peaks whose density contrast takes a value in $(\delta_L, \delta_L + d\delta_L)$ in a comoving volume is given by [29, 32]

$$n\left(\frac{\delta_L}{\sigma_L}\right) = \frac{\mu_L^3}{3^{3/2}4\pi^2\sigma_L^3} \left(\frac{\delta_L}{\sigma_L}\right)^3 e^{-\frac{\delta_L^2}{2\sigma_L^2}}, \quad (3.10)$$

where μ_L is given by

$$\mu_L^2 = \int_0^\infty \frac{dk}{k} k^2 \mathcal{P}_{\delta_L}(k) = \frac{16}{81} \int_0^\infty \frac{dk}{k} (kr_m)^4 \tilde{W}^2(k, r_m) k^2 \mathcal{P}_\zeta(k). \quad (3.11)$$

Using Eq.(3.10) in Eq.(3.9), we obtain

$$\beta(k_m) = \frac{1}{3^{3/2}\sqrt{2\pi}(aH)^3} \int_{\delta_{L-,c}}^{\delta_{\text{max}}} d\delta_L \left(\frac{M_{\text{PBH}}(\delta_L)}{M_H}\right) \left(\frac{\mu_L}{\sigma_L}\right)^3 \left(\frac{\delta_L}{\sigma_L}\right)^3 e^{-\frac{\delta_L^2}{2\sigma_L^2}}, \quad (3.12)$$

where we used $\delta_c = \delta_{L-,c}$ and $(aH)^{-3} = r_m^3$.

3.5 PBH mass in the critical phenomena

Before closing this section, let us briefly discuss the relation between M_{PBH} and the horizon mass M_H (which is proportional to the square of the horizon scale, $(aH)^{-2} = r_m^2$), which appears in the estimation of mass fraction parameter in Eq. (3.8) and Eq. (3.12). The final mass of the PBHs formed during the RD era, M_{PBH} depends on the initial density perturbation profile (i.e., shape and amplitude) and follows the scaling behaviour [52]

$$M_{\text{PBH}} = \kappa M_H (\delta - \delta_c)^\gamma = \kappa M_H \left[\delta_L - \frac{3}{8} \delta_L^2 - \delta_c \right]^\gamma \quad (3.13)$$

where κ (which we take 3 in this work) depends on the shape of the profile, $\gamma \simeq 0.36$ during RD epoch [40, 53]. This scaling behaviour holds approximately true up to M_H . The near-critical behaviour (3.13) shows that even if we consider perturbations of a single mode leading to

⁴The modified peak theory is also proposed in the literature [34] which differs only in the factor of $(aH)^{-4}$.

PBHs formation, the PBHs are formed in a finite mass range; and the monochromatic mass function is never realized. Nevertheless, the spread of the mass function is not significant and we may practically treat the resultant mass function as monochromatic one as long as the tail of the mass function, which only makes a subdominant contribution to the PBH abundance, is ignored. In what follows, we also consider the monochromatic mass function by assuming that all the PBHs have the same mass parametrized by a parameter α defined by $\alpha = M_{\text{PBH}}/M_H = \frac{4\pi}{3}\rho H^{-3}$.

Lastly, we should also note that when considering the constraints on monochromatic PBH mass function that are produced by a very narrow peaked power spectrum that peaks at a given wavenumber k_p , we can identify $r_m = 1/k_p$. This gives the PBHs mass fraction as a function of peak wavenumber, $\beta(k_p)$. Furthermore, we can relate this theoretical estimate with the constraints by using the mass-wavenumber relation [21]

$$M_{\text{PBH}}(k) \simeq 30M_\odot \left(\frac{\alpha}{0.2}\right)^{1/2} \left(\frac{g_*}{10.75}\right)^{-1/6} \left(\frac{k}{2.9 \times 10^5 \text{ Mpc}^{-1}}\right)^{-2}, \quad (3.14)$$

g_* is the number of relativistic degrees of freedom at the epoch of PBH formation.

4 Constraints on $\mathcal{P}_\zeta(k)$ from PBHs abundance

In this section, we derive model-independent (i.e., independent of the production mechanism of primordial perturbation) constraints on the primordial curvature power spectrum by using the PBH mass function derived in the previous section. We consider a generic form of the lognormal-type power spectrum, which can be parametrized as [54]

$$\mathcal{P}_\zeta(k) = \mathcal{A}_p \frac{1}{\sqrt{2\pi\Delta}} \exp\left(-\frac{\ln(k/k_p)^2}{2\Delta^2}\right), \quad (4.1)$$

where k_p and Δ are free parameters determining the position and the width of the peak, respectively. The overall normalization is determined by the amplitude \mathcal{A}_p which satisfies the condition $\int_0^\infty \mathcal{P}_\zeta(k) d\ln k = \mathcal{A}_p$. Furthermore, the scale-invariant power spectrum can be approximated as the infinitely broad peak limit $\Delta \rightarrow \infty$ while keeping $\mathcal{A}_p/\Delta = \text{constant}$, and the limit $\Delta \rightarrow 0$ gives the δ -function type peak as $\mathcal{P}_\zeta(k) = \mathcal{A}_p \delta(\ln(k/k_p))$. Note that the lognormal peak in the primordial curvature power spectrum can arise in many inflation models, for example, models predicting a very narrow peak in the primordial curvature power spectrum with $\Delta \ll 1$ are discussed in Refs.[6, 8, 55], and the models supporting the broad power spectrum with $\Delta \geq \mathcal{O}(1)$ are discussed in Refs.[3, 4, 7, 11, 13, 56]. Interestingly, it is shown in Ref.[29] that the PBH mass function remains approximately the same for $\Delta \lesssim 0.1$. Thus, we can use the lognormal power spectrum (4.1) with $\Delta = 0.1$ as the typical case for a monochromatic mass function of PBH.

4.1 Constraints on narrow peaked power spectrum from monochromatic PBH mass function

The narrow-peaked power spectrum produces all the PBHs with the same mass, which are described by a monochromatic mass function of PBHs. The constraints on PBHs' abundance for the monochromatic PBH mass function are presented in terms of the rescaled parameter β' , which is defined as [22]

$$\beta'(M) = \alpha^{1/2} \left(\frac{g_{*,i}}{106.75}\right)^{-1/4} \left(\frac{h}{0.67}\right)^{-2} \beta(M) \quad (4.2)$$

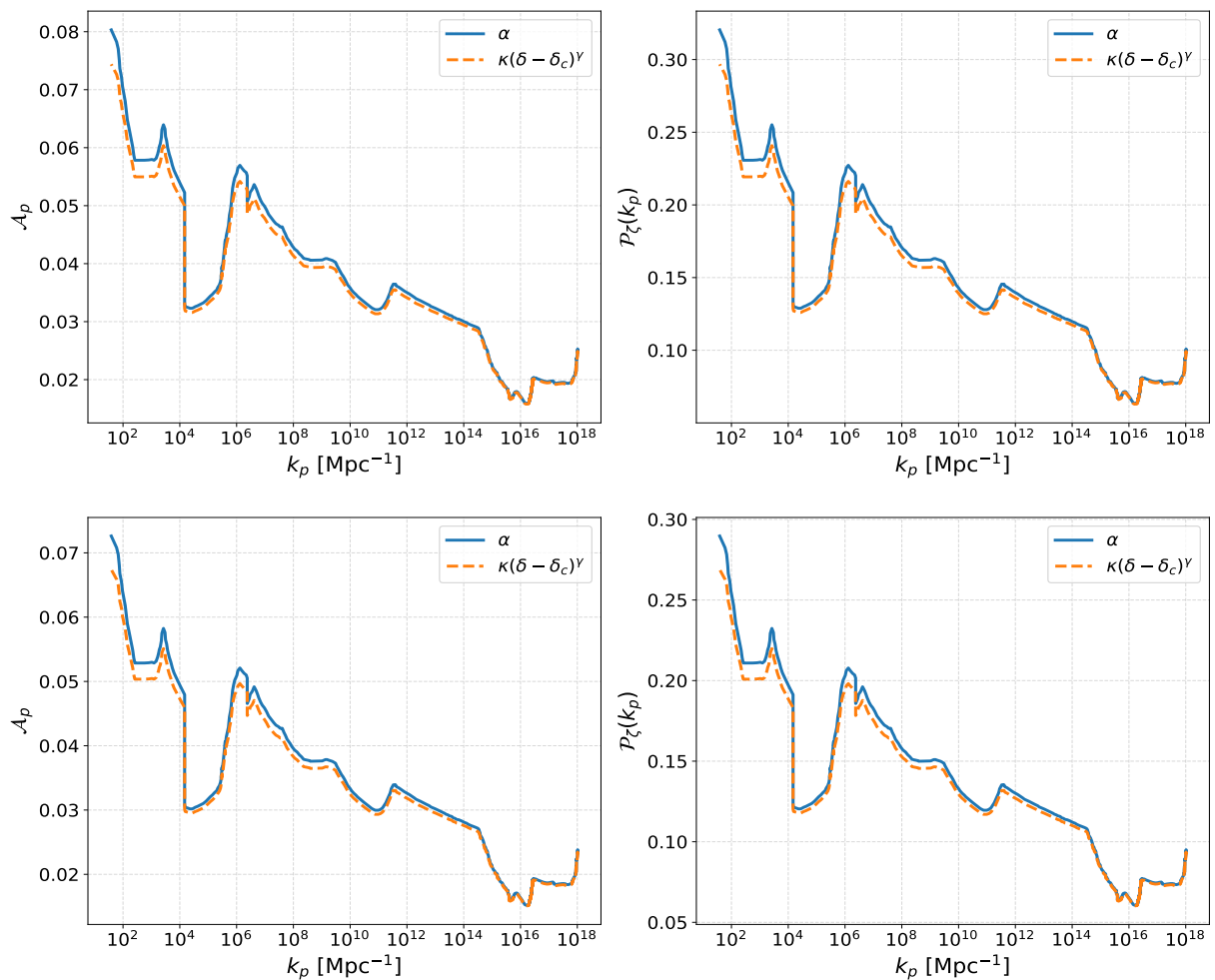


Figure 1. Showing the effect of the mass-ratio M_{PBH}/M_H on the amplitude \mathcal{A}_p and the lognormal power spectrum $\mathcal{P}_\zeta(k_p)$ for $\Delta = 0.1$ for spherical overdensity case. Solid curves are for constant value $\alpha = 0.2$ and dashed curves show the ratio obtained from the near-critical behaviour (3.13). The upper panel is for the PS formalism, and the lower panel is for the peak theory. In generating these plots, we choose $\alpha = 0.2$ in relation between β and β' in Eq.(4.2) in this work, and near-critical behaviour is assumed only inside the integration in the expression of β in Eq.(3.8) and Eq.(3.12).

where h is the uncertainty in Hubble parameter and $g_{*,i}$ is the number of relativistic degrees of freedom at the epoch of PBH formation⁵. Strictly speaking, the monochromatic mass function corresponds to the case where the mass-ratio, α is constant. Although α depends on the details of the gravitational collapse, we take $\alpha \simeq 0.2$, see the Ref. [21]. Another relation for the mass-ratio is determined by using the near-critical behavior in Eq.(3.13), which gives $\frac{M_{\text{PBH}}}{M_H} = \kappa(\delta - \delta_c)^\gamma$. Figure 1 shows the comparison between the effect of near-critical behavior with the $\alpha = 0.2$ case for spherical overdensity. Thus, we can see that for the monochromatic mass function of PBHs, the effect of near-critical relation is very small. Therefore, we show

⁵The advantage of using $\beta'(M) \approx 7.06 \times \Omega_{\text{PBH}}(M) \left(\frac{M}{10^{15} \text{g}}\right)^{1/2}$ instead of β as observational quantity is that it is independent of uncertainty in the values of $\alpha, h, g_{*,i}$, where $\Omega_{\text{PBH}} \equiv \rho_{\text{PBH}}(t_0)/\rho_{\text{critical}}$ is the PBH density parameter at present epoch.

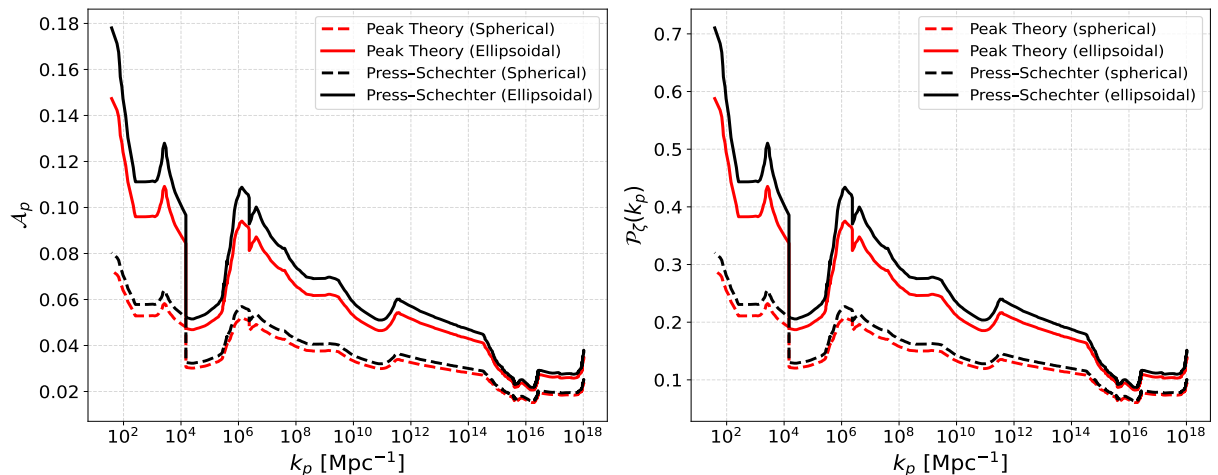


Figure 2. Showing comparison between Press-Schechter and peak theory on the constraints on \mathcal{A}_p and $\mathcal{P}_\zeta(k_p)$ for both spherical and ellipsoidal overdensity case, we use $\Delta = 0.1$ and $\alpha = 0.2$.

our final constraints from the monochromatic mass function for the case of $\alpha = 0.2$ only.

To obtain the constraints on the primordial curvature power spectrum, we use $\beta(k_p)$ derived in Eq. (3.8) within the PS formalism and in Eq. (3.12) within peak theory, and substitute these into the rescaled PBH mass fraction $\beta'(M)$ defined in Eq.(4.2). These expressions follow from the refined calculations based on the compaction function and incorporate the non-linear relation between the density contrast and the curvature perturbation. Using the most up-to-date constraints on the PBHs abundance from Ref. [22] together with the relation between PBHs mass and peak wavenumber in Eq.(3.14), we derive the corresponding constraints on the amplitude of the primordial curvature power spectrum assuming a monochromatic mass function. The results are shown in Figure 2, which compares the constraints obtained using the PS formalism and peak theory for both spherical and non-spherical (ellipsoidal) overdense regions. As expected, since the threshold density contrast for collapse is larger in the ellipsoidal case than in the spherical case, a larger amplitude of the power spectrum is required to produce the same PBH abundance. Some of these effects have been studied previously in the literature. For example, the comparison between the PS formalism and peak theory was investigated in Refs. [28, 29], while Ref. [27] considered the impact of non-sphericity within the PS formalism. However, these studies employed older PBH abundance constraints. Therefore, Fig. 2 presents updated and more robust constraints by comparing all of the above mentioned effects. Furthermore, in Figure 3, we compare our constraints (for the ellipsoidal case) on the amplitude of primordial power spectrum \mathcal{A}_p with the recent constraints from the LIGO-Virgo-KAGRA (LVK) O1-O4a runs [57], and the projected sensitivities of the Einstein Telescope (ET) and LIGO design (i.e., LIGO in its final phase).

4.2 Constraints on broad peaked power spectrum from extended PBHs mass function

Let us discuss the method for constraining the broad peak power spectrum, which leads to the production of PBHs with a relatively broader mass range referred to as the extended PBH mass function. Carr et al. proposed the method to obtain the constraints on any arbitrary mass function (or extended PBH mass function) from the constraints on monochromatic PBH

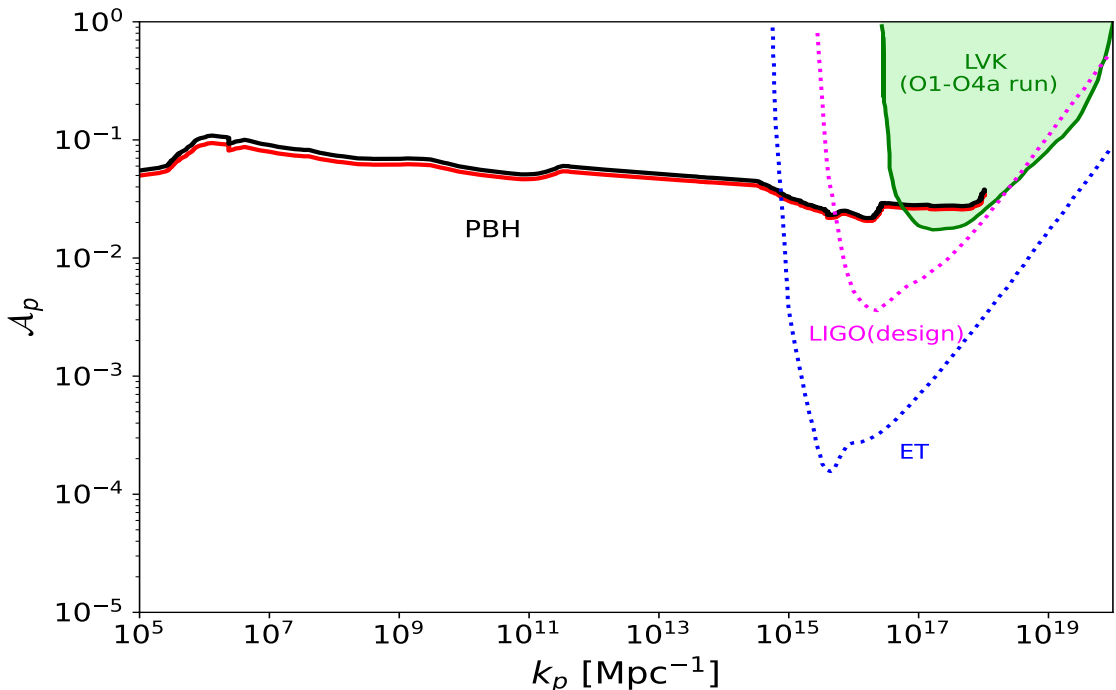


Figure 3. Comparison of our constraints (for ellipsoidal case) from Fig. 2 with other observational limits. The red and black curves show the constraints for peak theory and PS formalism, respectively. The solid Green line shows the region constrained by LVK O1 – O4a run [57]. The dotted magenta and blue curves show the projected sensitivities of the LIGO in its final phase (LIGO design) and the Einstein Telescope (ET), curves are taken from [58].

mass function [59]. Let us briefly review the method. We consider an astrophysical observable $A[\psi(M)]$ depending on the PBH abundance, which can be expanded as

$$A[\psi(M)] = A_0 + \int dM \psi(M) K_1(M) + \int dM_1 dM_2 \psi(M_1) \psi(M_2) K_2(M_1, M_2) + \dots, \quad (4.3)$$

where $\psi(M)$ is the PBH mass function, A_0 is the background contribution and the functions K_i depend on the details of the physics of observations. Assuming that the PBHs of different mass contribute independently to the astrophysical observable, we only need to consider the first two terms in Eq.(4.3). Thus, for the observational upper bound on the observable A_{obs} for a monochromatic mass function with $M_{\text{PBH}} = M_c$, the PBHs mass function becomes

$$\psi_{\text{mono}}(M_{\text{PBH}}) = f_{\text{PBH}}(M_c) \delta(M_{\text{PBH}} - M_c), \quad (4.4)$$

where f_{PBH} denotes the total PBH abundance relative to dark matter (to be discussed in detail later). This leads to the relation

$$f_{\text{PBH}}(M_c) \leq \frac{A_{\text{obs}} - A_0}{K_1(M_c)} \equiv f_{\text{max}}(M_c). \quad (4.5)$$

In the above equation f_{max} is the observationally allowed maxima of the fraction of DM in PBHs for a monochromatic mass distribution. Using Eq.(4.5) in Eq.(4.3), we have

$$\int dM \frac{\psi(M)}{f_{\text{max}}(M)} \leq 1, \quad (4.6)$$

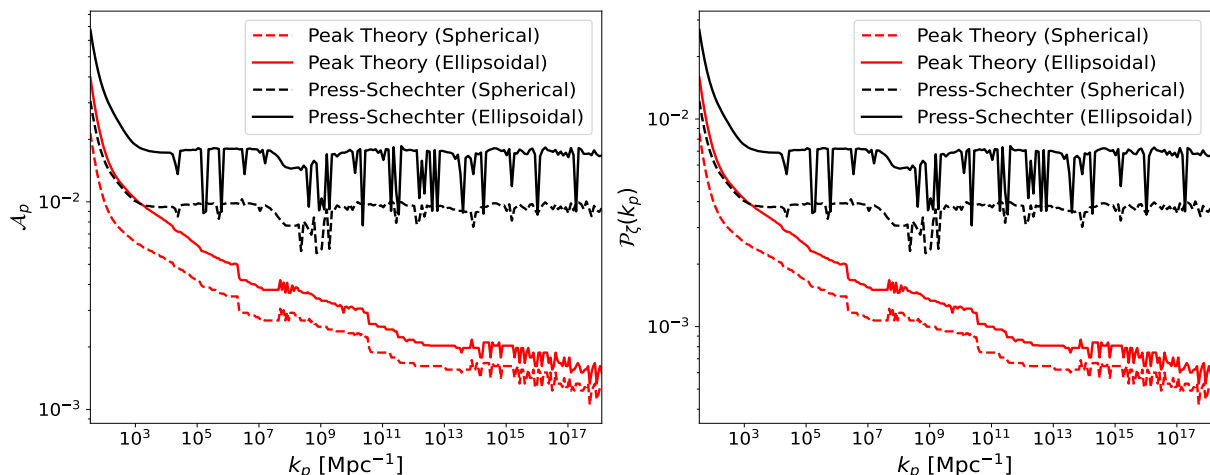


Figure 4. Showing comparison between Press-Schechter and peak theory on the constraints on \mathcal{A}_p and $\mathcal{P}_\zeta(k_p)$ for both spherical and ellipsoidal overdensity case, for broad peak case where we use $\Delta = 1$ and $\alpha = 0.2$. The constraints are obtained from the PBHs abundance against DM, f_{PBH} . The oscillatory behaviour for large k_p are the numerical artifact of rapidly oscillating $j_1^2(kr_m)$ term in σ_L^2 and μ_L^2 in Eqns.(3.7) and (3.11). The oscillating features are insignificant for the peak theory due to the effective cancellation between both terms in Eq.(3.12), while they become more prominent for PS formalism due to σ_L^2 dependence in Eq.(3.8).

which allows us to obtain the constraints on the arbitrary mass function $\psi(M)$ for a given f_{\max} . However, considering each of these N observables independently, the above procedure allows us to combine all the constraints by using the following relation [59]

$$\sum_{i=1}^N \left(\int dM \frac{\psi(M)}{f_{\max,i}(M)} \right)^2 \leq 1, \quad (4.7)$$

where $f_{\max,i}$ corresponds to different bounds for monochromatic mass function as defined by Eq.(4.5). Thus, the above relation provides the constraints on the arbitrary PBH mass function. However, we can instead use the combined monochromatic constraints from different observations provided in Ref.[22] over the entire mass range and use a more simplified relation given by [59]

$$\left(\int dM \frac{\psi(M)}{f_{\max}(M)} \right)^2 \leq 1. \quad (4.8)$$

We use the above relation to derive the constraints on the broad power spectrum. In the above equation, the numerator and denominator in integrand are provided by the theoretical model and observational bounds, respectively.

Using the PBHs mass function Eq.(3.4) in Eq.(4.8), we derive the constraints on the broad peak primordial power spectrum $\mathcal{P}_\zeta(k_p)$ for $\Delta = 1$. The constraints⁶ for both PS and peak theory are shown in Figure 4. Similar to the monochromatic case, we can see that the amplitude of the primordial power spectrum is larger for the ellipsoidal case. However, the raw

⁶The constraints in Figures 4 and 5 are derived from the PBH abundance relative to dark matter f_{PBH} , which is related to the initial abundance $\beta'(M)$ through $f_{PBH} = 2.7 \times 10^8 (M/M_\odot)^{-1/2} \beta'(M)$.

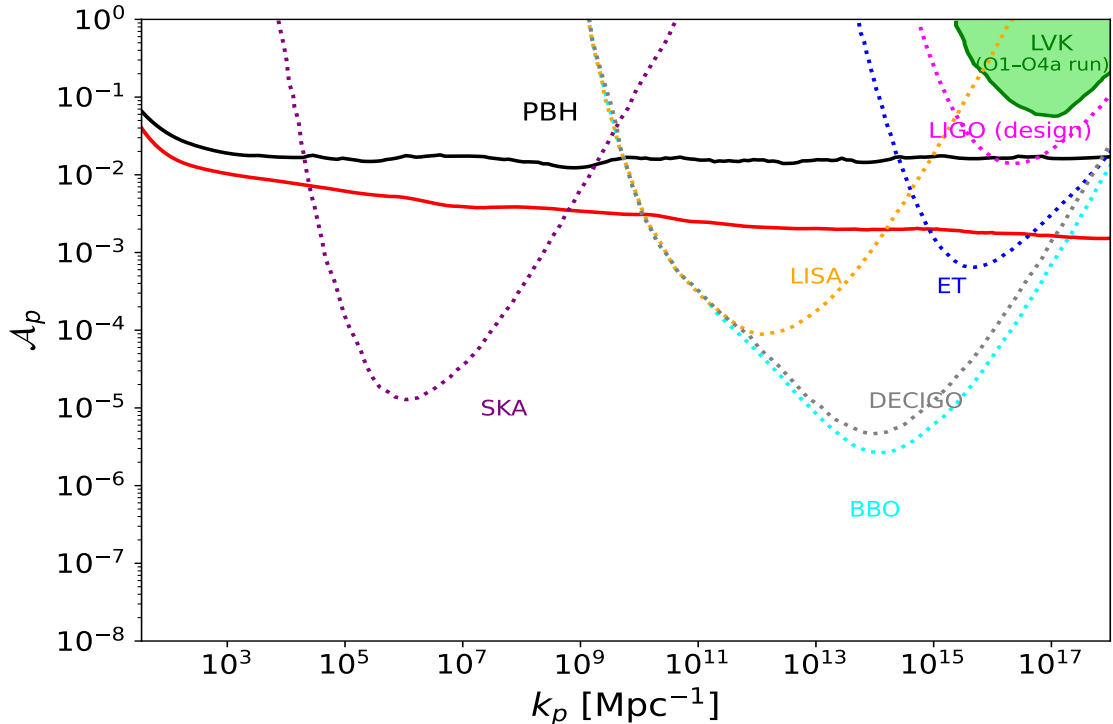


Figure 5. Comparison of our constraints (for ellipsoidal case) from Fig. 4 with other observational limits. The red and black curves show the constraints for peak theory and PS formalism, respectively. The solid Green line shows the region constrained by LVK *O1 – O4a* run [57]. The dotted curves show the projected sensitivities of the LIGO in its final phase (LIGO design) and the ET, SKA, BBO, DECIGO, LISA, which are taken from [58, 67].

numerical constraints contain spiky features arising from numerical artifacts. To remove these unphysical fluctuations, we smooth the data using the Savitzky–Golay filter, a commonly used method for suppressing noise while preserving the underlying trend. The resulting smoothed constraints are shown in Figure. 5. In this figure, we also compare our constraints with other observations probing small-scale primordial power spectrum, such as LIGO-Virgo-KAGRA (LVK) *O1-O4a* runs [57], ET [60, 61], Square Kilometer Array (SKA) [61, 62], Big Bang Observer (BBO) [63, 64], DECI-hertz Interferometer Gravitational-wave Observatory (DECIGO) [65], Laser Interferometer Space Antenna (LISA) [64, 66]. Interestingly, in contrast to the monochromatic case, we find that the constraints on the amplitude of a broad primordial power spectrum differ significantly between the PS formalism and peak theory, with the discrepancy becoming increasingly pronounced toward smaller scales (i.e., larger wavenumbers). From Eq.(3.12), we can see that because $\mu_L^2(k)$ is sensitive to small scales (as compared to $\sigma_L^2(k)$), the constraints for broad peak case for peak theory are expected to differ from PS formalism (which only depends on $\sigma_L^2(k)$). This reveals an important feature of the broad-spectrum case that has not been previously emphasized in the literature. Given the current lack of consensus on the definitive method for deriving the PBH mass function from a primordial power spectrum, the discrepancy between the black and red curves in Fig. 5 illustrates the magnitude of these theoretical uncertainties. This highlights the critical need for further studies to establish a more reliable computational framework.

5 Conclusion

Constraints on the abundance of PBHs provide a unique opportunity to constrain the primordial power spectrum (\mathcal{P}_ζ) at small scales, regimes which are not probed by standard cosmological observations like the CMB and galaxy surveys. This connection is established via the PBH formation mechanism, which relies on the collapse of large-amplitude primordial curvature perturbations at the time of the horizon re-entry during RD epoch. Crucially, deriving stringent limits requires the precise and careful modeling of the nonlinear dynamics of the collapse of density perturbations leading to PBH formation in the early Universe.

In this work, we revisited and refined the methodology to translate the PBH abundance bounds into upper-limits on the primordial curvature power spectrum, thereby placing this connection on a more solid theoretical footing. Using the most up-to-date constraints on PBH abundances, we systematically investigated multiple sources of theoretical uncertainty that affect PBH formation and their resulting mass function. Employing refined calculations based on the compaction function and accounting for the full nonlinear relation between curvature perturbations and density contrast, we compared the resulting constraints across key modeling choices, including the PS formalism versus peak theory and monochromatic versus extended PBH mass functions, while also assessing the impact of spherical versus ellipsoidal collapse criteria for overdense regions. Although several of these effects have been examined individually in earlier works, to our knowledge, this is the first detailed study that incorporates all of them within a single, unified framework to evaluate their combined impact on the inferred primordial power spectrum. Our results showed that the amplitude of primordial power spectrum (for both narrow and broad peak) required for the PBHs formation is larger when non-spherical collapse is included, owing to the higher threshold density contrast. By incorporating various effects coherently, our analysis provides more robust, precise upper limits on both narrow and broad peak primordial curvature power spectra. These results not only refine the constraints on PBH scenarios but also strengthen the use of PBH abundance as an indirect probe of the final stages of inflation, particularly on smaller scales inaccessible to other cosmological observations. In Figures 3 and 5, we also compared our constraints with other observations. Notably, we found that the constraints derived using the PS formalism and peak theory differ significantly toward smaller scales in the case of a broad primordial power spectrum, whereas they remain largely consistent for the monochromatic case.

A Calculations on relating volume average density contrast with smoothed density contrast

In this appendix, we show that the volume average and smoothing (with top-hat window function in real space) of the density contrast (i.e., $\delta\rho/\bar{\rho}$) are essentially the same quantities if the radius of volume is equal to the smoothing scale. Let us consider the relation for the volume average density contrast which is defined as the volume average of $\delta\rho/\bar{\rho}$ over the radius of sphere of volume R_m as

$$\delta_{\text{average}}(r_m, t) = \frac{1}{V_m} \int_0^{R_m} dR 4\pi R^2 \frac{\delta\rho}{\bar{\rho}} \quad (\text{A.1})$$

where we integrated over the volume $V_m = \frac{4\pi R_m^3}{3}$. Alternatively, we can also define the above relation as the smoothing over the top-hat window function in real space in the following way

$$\delta_{\text{smooth}}(r_m, t) = \int dR 4\pi R^2 \frac{\delta\rho}{\bar{\rho}} W_{\text{TH}}(R_m, R) = \int dR 4\pi R^2 \frac{\delta\rho}{\bar{\rho}} \frac{3}{4\pi R_m^3} \Theta(R_m - R) \quad (\text{A.2})$$

where $W_{\text{TH}}(R_m, R) = \frac{3}{4\pi R_m^3} \Theta(R_m - R)$ is the top-hat window function in real space, and $\Theta(R_m - R)$ is the Heaviside theta function with the following values: $\Theta(R_m - R) = 1$ for $R < R_m$ and $\Theta(R_m - R) = 0$ for $R > R_m$. Therefore, the values of the Theta function constrain the integration range to be $0 < R < R_m$ and we obtain (A.2) as

$$\delta_{\text{smooth}}(r_m, t) = \int_0^{R_m} dR 4\pi R^2 \frac{\delta\rho}{\bar{\rho}} \frac{3}{4\pi R_m^3} = \frac{1}{V_m} \int_0^{R_m} dR 4\pi R^2 \frac{\delta\rho}{\bar{\rho}} = \delta_{\text{average}}(r_m, t) \quad (\text{A.3})$$

where we substituted $\Theta(R_m - R) = 1$, and used Eq.(A.1) in the last equality. Therefore, in our case both are the same and are denoted as $\delta_m = \delta_{\text{average}}(r_m) = \delta_{\text{smooth}}(r_m)$.

Acknowledgments

The work of A.K. was supported by the Japan Society for the Promotion of Science (JSPS) as part of the JSPS Postdoctoral Program (Grant Number: 25KF0107). T.S. gratefully acknowledges support from JSPS KAKENHI grant (Grant Number JP23K03411).

References

- [1] Scott Dodelson and Fabian Schmidt. *Modern Cosmology*. 2020.
- [2] Daniel Baumann. *Cosmology*. Cambridge University Press, 7 2022.
- [3] Juan Garcia-Bellido, Andrei D. Linde, and David Wands. Density perturbations and black hole formation in hybrid inflation. *Phys. Rev. D*, 54:6040–6058, 1996.
- [4] Jun'ichi Yokoyama. Chaotic new inflation and formation of primordial black holes. *Phys. Rev. D*, 58:083510, 1998.
- [5] Kazunori Kohri, David H. Lyth, and Alessandro Melchiorri. Black hole formation and slow-roll inflation. *JCAP*, 04:038, 2008.
- [6] Masahiro Kawasaki, Naoya Kitajima, and Tsutomu T. Yanagida. Primordial black hole formation from an axionlike curvaton model. *Phys. Rev. D*, 87(6):063519, 2013.
- [7] Juan Garcia-Bellido and Ester Ruiz Morales. Primordial black holes from single field models of inflation. *Phys. Dark Univ.*, 18:47–54, 2017.
- [8] Keisuke Inomata, Masahiro Kawasaki, Kyohei Mukaida, Yuichiro Tada, and Tsutomu T. Yanagida. Inflationary Primordial Black Holes as All Dark Matter. *Phys. Rev. D*, 96(4):043504, 2017.
- [9] Bernard Carr, Konstantinos Dimopoulos, Charlotte Owen, and Tommi Tenkanen. Primordial Black Hole Formation During Slow Reheating After Inflation. *Phys. Rev. D*, 97(12):123535, 2018.
- [10] Christian T. Byrnes, Philippa S. Cole, and Subodh P. Patil. Steepest growth of the power spectrum and primordial black holes. *JCAP*, 06:028, 2019.
- [11] Keisuke Inomata, Masahiro Kawasaki, Kyohei Mukaida, and Tsutomu T. Yanagida. Double inflation as a single origin of primordial black holes for all dark matter and LIGO observations. *Phys. Rev. D*, 97(4):043514, 2018.

- [12] Nilanjandev Bhaumik and Rajeev Kumar Jain. Primordial black holes dark matter from inflection point models of inflation and the effects of reheating. JCAP, 01:037, 2020.
- [13] Matteo Braglia, Dhiraj Kumar Hazra, Fabio Finelli, George F. Smoot, L. Sriramkumar, and Alexei A. Starobinsky. Generating PBHs and small-scale GWs in two-field models of inflation. JCAP, 08:001, 2020.
- [14] H. V. Ragavendra, Pankaj Saha, L. Sriramkumar, and Joseph Silk. Primordial black holes and secondary gravitational waves from ultraslow roll and punctuated inflation. Phys. Rev. D, 103(8):083510, 2021.
- [15] Ya. B. Zel’dovich and I. D. Novikov. The Hypothesis of Cores Retarded during Expansion and the Hot Cosmological Model. Sov. Astron., 10:602, 1967.
- [16] Stephen Hawking. Gravitationally collapsed objects of very low mass. Mon. Not. Roy. Astron. Soc., 152:75, 1971.
- [17] Bernard J. Carr and S. W. Hawking. Black holes in the early Universe. Mon. Not. Roy. Astron. Soc., 168:399–415, 1974.
- [18] George F. Chapline. Cosmological effects of primordial black holes. Nature, 253(5489):251–252, 1975.
- [19] Maxim Yu. Khlopov. Primordial Black Holes. Res. Astron. Astrophys., 10:495–528, 2010.
- [20] Bernard Carr, Florian Kuhnel, and Marit Sandstad. Primordial black holes as dark matter. Phys. Rev. D, 94(8):083504, 2016.
- [21] Misao Sasaki, Teruaki Suyama, Takahiro Tanaka, and Shuichiro Yokoyama. Primordial black holes—perspectives in gravitational wave astronomy. Class. Quant. Grav., 35(6):063001, 2018.
- [22] Bernard Carr, Kazunori Kohri, Yuuiti Sendouda, and Jun’ichi Yokoyama. Constraints on primordial black holes. Reports on Progress in Physics, 84(11):116902, dec 2021.
- [23] Anne M. Green and Bradley J. Kavanagh. Primordial Black Holes as a dark matter candidate. J. Phys. G, 48(4):043001, 2021.
- [24] Albert Escrivà, Florian Kuhnel, and Yuichiro Tada. Primordial Black Holes. 11 2022.
- [25] Guillem Domènech, Shi Pi, and Ao Wang. A Unified Origin of Primordial Black Hole Dark Matter and Nanohertz Gravitational Waves. 2 2026.
- [26] Ashu Kushwaha and Teruaki Suyama. Constraining small-scale primordial magnetic fields from the abundance of primordial black holes. JCAP, 12:012, 2024.
- [27] Gabriela Sato-Polito, Ely D. Kovetz, and Marc Kamionkowski. Constraints on the primordial curvature power spectrum from primordial black holes. Phys. Rev. D, 100(6):063521, 2019.
- [28] Alba Kalaja, Nicola Bellomo, Nicola Bartolo, Daniele Bertacca, Sabino Matarrese, Ilia Musco, Alvise Raccanelli, and Licia Verde. From Primordial Black Holes Abundance to Primordial Curvature Power Spectrum (and back). JCAP, 10:031, 2019.
- [29] Andrew D. Gow, Christian T. Byrnes, Philippa S. Cole, and Sam Young. The power spectrum on small scales: Robust constraints and comparing PBH methodologies. JCAP, 02:002, 2021.
- [30] William H. Press and Paul Schechter. Formation of Galaxies and Clusters of Galaxies by Self-Similar Gravitational Condensation. ApJ, 187:425–438, February 1974.
- [31] James M. Bardeen, J. R. Bond, Nick Kaiser, and A. S. Szalay. The Statistics of Peaks of Gaussian Random Fields. Astrophys. J., 304:15–61, 1986.
- [32] Sam Young, Christian T. Byrnes, and Misao Sasaki. Calculating the mass fraction of primordial black holes. JCAP, 07:045, 2014.

- [33] Chul-Moon Yoo, Tomohiro Harada, Shin'ichi Hirano, and Kazunori Kohri. Abundance of Primordial Black Holes in Peak Theory for an Arbitrary Power Spectrum. PTEP, 2021(1):013E02, 2021. [Erratum: PTEP 2024, 049203 (2024)].
- [34] Sam Young and Marcello Musso. Application of peaks theory to the abundance of primordial black holes. JCAP, 11:022, 2020.
- [35] Florian Kühnel and Marit Sandstad. Ellipsoidal collapse and primordial black hole formation. Phys. Rev. D, 94(6):063514, 2016.
- [36] Ignacio Zaballa, Anne M. Green, Karim A. Malik, and Misao Sasaki. Constraints on the primordial curvature perturbation from primordial black holes. JCAP, 03:010, 2007.
- [37] Edgar Bugaev and Peter Klimai. Constraints on amplitudes of curvature perturbations from primordial black holes. Phys. Rev. D, 79:103511, 2009.
- [38] Zhu Yi and Qin Fei. Constraints on primordial curvature spectrum from primordial black holes and scalar-induced gravitational waves. Eur. Phys. J. C, 83(1):82, 2023.
- [39] Ilija Musco. Threshold for primordial black holes: Dependence on the shape of the cosmological perturbations. Phys. Rev. D, 100(12):123524, 2019.
- [40] Sam Young, Ilija Musco, and Christian T. Byrnes. Primordial black hole formation and abundance: contribution from the non-linear relation between the density and curvature perturbation. JCAP, 11:012, 2019.
- [41] Cristiano Germani and Ilija Musco. Abundance of primordial black holes depends on the shape of the inflationary power spectrum. Phys. Rev. Lett., 122(14):141302, 2019.
- [42] Masaru Shibata and Misao Sasaki. Black hole formation in the Friedmann universe: Formulation and computation in numerical relativity. Phys. Rev. D, 60:084002, 1999.
- [43] Ilija Musco. Threshold for primordial black holes: Dependence on the shape of the cosmological perturbations. Phys. Rev. D, 100(12):123524, 2019.
- [44] Tomohiro Harada, Chul-Moon Yoo, and Yasutaka Koga. Revisiting compaction functions for primordial black hole formation. Phys. Rev. D, 108(4):043515, 2023.
- [45] Tomohiro Harada, Hayami Iizuka, Yasutaka Koga, and Chul-Moon Yoo. Geometrical origin for the compaction function for primordial black hole formation. Phys. Rev. D, 111(2):023537, 2025.
- [46] Sam Young. Computation of the Abundance of Primordial Black Holes. 2025.
- [47] Koichiro Uehara, Albert Escrivà, Tomohiro Harada, Daiki Saito, and Chul-Moon Yoo. Numerical simulation of type II primordial black hole formation. JCAP, 01:003, 2025.
- [48] Albert Escrivà and Chul-Moon Yoo. Simulations of ellipsoidal primordial black hole formation. Phys. Rev. D, 112(8):083518, 2025.
- [49] Albert Escrivà and Chul-Moon Yoo. Nonspherical effects on the mass function of primordial black holes. Phys. Rev. D, 112(8):L081304, 2025.
- [50] B. J. Carr, Kazunori Kohri, Yuuiti Sendouda, and Jun'ichi Yokoyama. New cosmological constraints on primordial black holes. Phys. Rev. D, 81:104019, 2010.
- [51] Ashu Kushwaha and Teruaki Suyama. Excursion Set Approach to Primordial Black Holes: Cloud-in-Cloud and Mass Function Revisited. 9 2025.
- [52] Jens C. Niemeyer and K. Jedamzik. Near-critical gravitational collapse and the initial mass function of primordial black holes. Phys. Rev. Lett., 80:5481–5484, 1998.
- [53] Charles R. Evans and Jason S. Coleman. Observation of critical phenomena and selfsimilarity in the gravitational collapse of radiation fluid. Phys. Rev. Lett., 72:1782–1785, 1994.

- [54] Shi Pi and Misao Sasaki. Gravitational Waves Induced by Scalar Perturbations with a Lognormal Peak. *JCAP*, 09:037, 2020.
- [55] M. Kawasaki, N. Sugiyama, and T. Yanagida. Primordial black hole formation in a double inflation model in supergravity. *Phys. Rev. D*, 57:6050–6056, 1998.
- [56] Sébastien Clesse and Juan García-Bellido. Massive Primordial Black Holes from Hybrid Inflation as Dark Matter and the seeds of Galaxies. *Phys. Rev. D*, 92(2):023524, 2015.
- [57] A. G. Abac et al. Cosmological and High Energy Physics implications from gravitational-wave background searches in LIGO-Virgo-KAGRA’s O1-O4a runs. 10 2025.
- [58] Alba Romero-Rodriguez, Mario Martinez, Oriol Pujolàs, Mairi Sakellariadou, and Ville Vaskonen. Search for a Scalar Induced Stochastic Gravitational Wave Background in the Third LIGO-Virgo Observing Run. *Phys. Rev. Lett.*, 128(5):051301, 2022.
- [59] Bernard Carr, Martti Raidal, Tommi Tenkanen, Ville Vaskonen, and Hardi Veermäe. Primordial black hole constraints for extended mass functions. *Phys. Rev. D*, 96(2):023514, 2017.
- [60] B. S. Sathyaprakash and B. F. Schutz. Physics, Astrophysics and Cosmology with Gravitational Waves. *Living Rev. Rel.*, 12:2, 2009.
- [61] C. J. Moore, R. H. Cole, and C. P. L. Berry. Gravitational-wave sensitivity curves. *Class. Quant. Grav.*, 32(1):015014, 2015.
- [62] Gemma Janssen et al. Gravitational wave astronomy with the SKA. *PoS*, AASKA14:037, 2015.
- [63] Kent Yagi and Naoki Seto. Detector configuration of DECIGO/BBO and identification of cosmological neutron-star binaries. *Phys. Rev. D*, 83:044011, 2011. [Erratum: *Phys.Rev.D* 95, 109901 (2017)].
- [64] Eric Thrane and Joseph D. Romano. Sensitivity curves for searches for gravitational-wave backgrounds. *Phys. Rev. D*, 88(12):124032, 2013.
- [65] Sachiko Kuroyanagi, Kazunori Nakayama, and Jun’ichi Yokoyama. Prospects of determination of reheating temperature after inflation by DECIGO. *PTEP*, 2015(1):013E02, 2015.
- [66] Pau Amaro-Seoane, Heather Audley, Stanislav Babak, John Baker, Enrico Barausse, Peter Bender, Emanuele Berti, Pierre Binetruy, Michael Born, Daniele Bortoluzzi, Jordan Camp, Chiara Caprini, Vitor Cardoso, Monica Colpi, John Conklin, Neil Cornish, Curt Cutler, Karsten Danzmann, Rita Dolesi, Luigi Ferraioli, Valerio Ferroni, Ewan Fitzsimons, Jonathan Gair, Lluís Gesa Bote, Domenico Giardini, Ferran Gibert, Catia Grimani, Hubert Halloin, Gerhard Heinzl, Thomas Hertog, Martin Hewitson, Kelly Holley-Bockelmann, Daniel Hollington, Mauro Hueller, Henri Inchauspe, Philippe Jetzer, Nikos Karnesis, Christian Killow, Antoine Klein, Bill Klipstein, Natalia Korsakova, Shane L Larson, Jeffrey Livas, Ivan Lloro, Nary Man, Davor Mance, Joseph Martino, Ignacio Mateos, Kirk McKenzie, Sean T McWilliams, Cole Miller, Guido Mueller, Germano Nardini, Gijs Nelemans, Miquel Nofrarias, Antoine Petiteau, Paolo Pivato, Eric Plagnol, Ed Porter, Jens Reiche, David Robertson, Norna Robertson, Elena Rossi, Giuliana Russano, Bernard Schutz, Alberto Sesana, David Shoemaker, Jacob Slutsky, Carlos F. Sopuerta, Tim Sumner, Nicola Tamanini, Ira Thorpe, Michael Troebs, Michele Vallisneri, Alberto Vecchio, Daniele Vetrugno, Stefano Vitale, Marta Volonteri, Gudrun Wanner, Harry Ward, Peter Wass, William Weber, John Ziemer, and Peter Zweifel. Laser Interferometer Space Antenna. *arXiv e-prints*, page arXiv:1702.00786, February 2017.
- [67] Keisuke Inomata and Tomohiro Nakama. Gravitational waves induced by scalar perturbations as probes of the small-scale primordial spectrum. *Phys. Rev. D*, 99(4):043511, 2019.